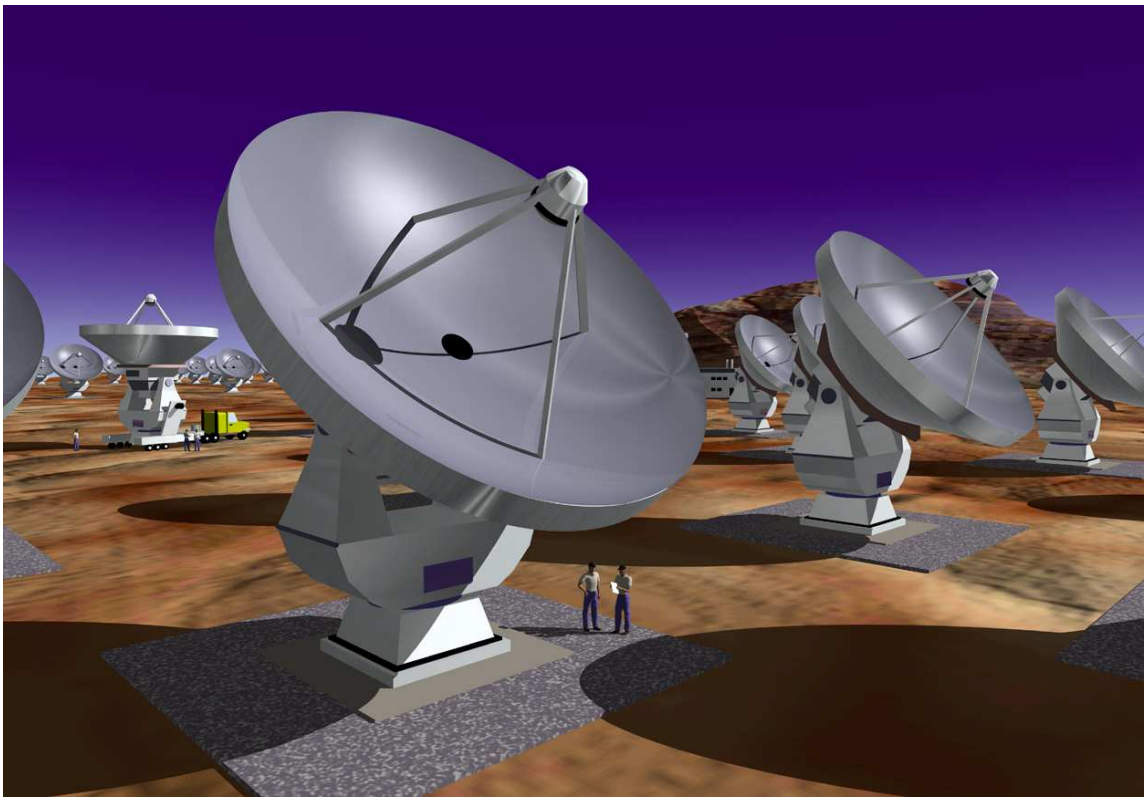

Atacama Large Millimeter Array

ALMA Memo 434

Load Calibration at Millimeter and Submillimeter Wavelengths

Jeff Mangum (NRAO Tucson)

October 17, 2002

Abstract

Accurate amplitude calibration at millimeter and submillimeter wavelengths is a difficult goal to achieve due to the temporal variability of the emissive and absorptive properties of the Earth's atmosphere and the lack of an accurate astronomical flux standard. The difficulties with deriving a uniform amplitude calibration system has resulted in the three step calibration process used at millimeter and submillimeter single dishes and interferometers. The second step in this process involves the *chopper wheel calibration technique*. Chopper wheel calibration is used to derive the antenna temperature of an astronomical source corrected for atmospheric extinction. An analysis of the uncertainties in three variants of this technique, two which use a single calibrated load and a third which uses two calibrated loads, has been derived. The conclusion of this analysis is that the one-load chopper calibration systems are more uncertain than the two-load chopper calibration system. This is especially true at submillimeter wavelengths. The main reason for the larger uncertainty of the one-load chopper calibration systems is the fact that they require a knowledge of the mean atmospheric temperature, which is inherently difficult to obtain. Of the two calibration systems, the two-load chopper system has the potential for reaching a calibration accuracy of approximately 1% for all bands, as specified for the ALMA receiving systems.

1 Introduction

Over the last 30 years considerable effort has been devoted to the development of an absolute calibration technique for millimeter astronomical measurements. The three most significant problems which one must overcome when calibrating the amplitude of millimeter astronomical measurements are:

- Implementation of a stable total power system;
- The variable attenuation of millimeter signals due to the Earth's atmosphere. This opacity is due primarily to the combined absorptive and emissive effects of O_2 and H_2O;
- The lack of an appropriate astronomical amplitude calibration source.

In the following, we describe the amplitude calibration scheme used at millimeter and submillimeter wavelengths and address the needs for accurate amplitude calibration for ALMA. In this analysis, we consider most sources of uncertainty **except** uncertainty due to:

- pointing errors,
- variations in the antenna beam pattern with time and elevation,
- loss of correlation due to atmospheric or instrumental phase noise, and
- gain compression in the SIS mixer or amplifiers.

2 The Amplitude Calibration Ladder

A graphical description of the "calibration ladder" used at millimeter and submillimeter wavelengths is shown in Figure 1. The uncertainties associated with each step of the ladder are typical of the current calibration systems used at existing millimeter wavelength observatories. The target uncertainties for amplitude calibration with ALMA are listed in parentheses for each step.

The first step of the amplitude calibration ladder is the easiest of the three steps to derive. Good gain stability, to a level of at least 1% over time scales less than approximately 10 seconds, are relatively easy to maintain with well-built receiving systems. The gain stability specification for ALMA is 10^{-4} over time scales $\leq$1 second.

The second step in this amplitude calibration ladder, the calibration of the telescope-dependent amplitude scale, is an inherently difficult task to accomplish. For most astronomical measurements this calibration step is accomplished through the measurement of a noise source of known emissive properties. At centimeter wavelengths the common noise source used for calibration is a waveguide oscillator or diode which emits a broad-band noise source directly into the radio receiver. At shorter wavelengths, noise tube or diode calibration sources become problematic to use due to their frequency-, time-, and

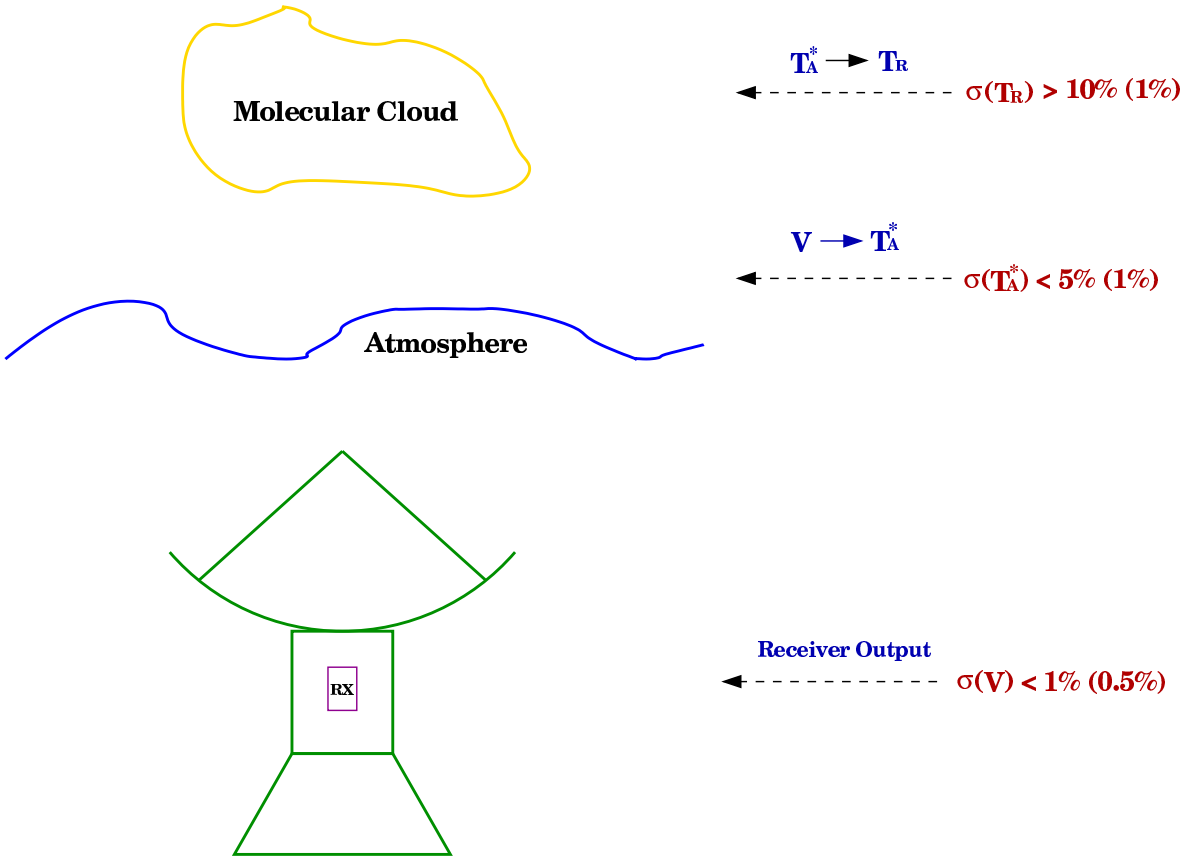

Figure 1: Graphical representation of the "calibration ladder" used at millimeter and submillimeter wavelengths. The current state of the art for determining each step of the ladder is indicated, along with the ALMA requirements for each in parentheses. The chopper wheel calibration technique is used to determine the second step in this ladder.

polarization-dependent output characteristics. The difficulties encountered in applying noise tube calibration to millimeter astronomical measurements lead Penzias & Burrus (1973) to develop the chopper wheel calibration technique. In this technique, the response of the receiver is calibrated by alternately introducing and removing black body absorbers of known or estimated physical temperature at a convenient point in the signal path of the receiver. The calibrating noise signal is then the difference between the temperatures of these absorbers. The broad band and frequency independent emissive properties of the absorbers, coupled with the simplicity and reliability of this technique, has resulted in its adoption as the main calibration system used at most radio observatories which operate at millimeter wavelengths.

The chopper wheel calibration technique allows for the conversion of measured voltages at the receiver to an antenna temperature corrected for the time- and position-variable emissive properties of the Earth's atmosphere. In the following, we investigate the accuracy of three forms of the chopper wheel calibration technique when applied to observations at millimeter and submillimeter wavelengths. Definitions for the terms used in this analysis can be found in Appendix A.

3 Terms Used in the T_A^* Temperature Scale

The received signals from the sky, load, and source measurements are given by

$$\begin{aligned} V_{sky} &= K\left(G_s J^s_{sky} + G_i J^i_{sky} + T_{rx}\right) + V_{offset} \\ &= K\Big[G_s\left(J^s_{sky-cold} + J^s_{sky-hot} + J^s_{ant} + \eta_l J^s_{bg}\exp(-\tau_s)\right) + \\ &\quad G_i\left(J^i_{sky-cold} + J^i_{sky-hot} + J^i_{ant} + \eta_l J^i_{bg}\exp(-\tau_i)\right) + T_{rx}\Big] + V_{offset} \\ &= K\Big[G_s\left[\eta_l J^s_m\left(1-\exp(-\tau_s)\right) + \left(1-\eta_l\right)J^s_{spill} + \eta_l J^s_{bg}\exp(-\tau_s)\right] + \\ &\quad G_i\left(\eta_l J^i_m\left[1-\exp(-\tau_i)\right] + \left(1-\eta_l\right)J^i_{spill} + \eta_l J^i_{bg}\exp(-\tau_i)\right) + T_{rx}\Big] + V_{offset} \end{aligned} \quad (1)$$

$$V_{load} = Kf\left[G_s J^s_{load} + G_i J^i_{load}\right] + KT_{rx} + V_{offset} \quad (2)$$

$$\begin{aligned} V_{source} &= K\left[G_s J^s_{A-sky} + G_i J^i_{A-sky} + T_A(source) + T_{rx}\right] + V_{offset} \\ &= K\left[G_s J^s_{A-sky} + G_i J^i_{A-sky} + \eta_l\left[T^*_{As} G_s\exp(-\tau_s) + T^*_{Ai} G_i\exp(-\tau_i)\right] + T_{rx}\right] \\ &\quad + V_{offset} \end{aligned} \quad (3)$$

Note that Equation 1 is equivalent to Equation 3 in Ulich & Haas (1976). Using the definitions for V_{sky} (Equation 1), V_{load} (Equation 2), and V_{source} (Equation 3), and noting that

$$V_{source} - V_{sky} = K\eta_l\left[T^*_{As} G_s\exp(-\tau_s) + T^*_{Ai} G_i\exp(-\tau_i)\right] \quad (4)$$

we can assume that the signal to be observed exists only in the signal sideband (so that $T^*_{As} = T^*_A$) to derive the standard equation for T^*_A

$$\boxed{T^*_A = \frac{V_{source} - V_{sky}}{K G_s \eta_l \exp(-\tau_s)}} \tag{5}$$

A common calibration factor used to quantify millimeter and submillimeter measurements acquired with both single dish and interferometric techniques is the system temperature T_{sys}, which is defined as

$$T_{sys} \equiv \frac{V_{sky}}{V_{source} - V_{sky}} \left(T^*_{As} + T^*_{Ai}\right) \tag{6}$$

Using Equations 1, 3, and 5, Equation 6 becomes

$$T_{sys} = \frac{G_s J^s_{A-sky} + G_i J^i_{A-sky} + T_{rx}}{\eta_l \left[T^*_{As} G_s \exp(-\tau_s) + T^*_{Ai} G_i \exp(-\tau_i)\right]} \left[T^*_{As} + T^*_{Ai}\right] \tag{7}$$

If we are only interested in signals which come from the signal sideband, then $T^*_{Ai} = 0$. Therefore, with $T^*_{As} = T^*_A$, Equation 7 becomes

$$T_{sys} = \frac{J^s_{A-sky} + T_{rx}}{G_s \eta_l \exp(-\tau_s)} \tag{8}$$

Note that Equation 8 requires a measurement of T_{rx}, which is derived from sequential measurements of two calibrated loads at known temperatures T_{load1} and T_{load2}

$$\begin{aligned} T_{rx} &= \frac{J_{load1} V_{load2} - J_{load2} V_{load1}}{V_{load1} - V_{load2}} \\ &= \frac{J_{load1} - Y J_{load2}}{Y - 1} \end{aligned} \tag{9}$$

where $Y \equiv \frac{V_{load1}}{V_{load2}}$.

4 Derivation and Calibration of the T^*_A Temperature Scale

Proper scaling of the T^*_A and T_{sys} temperatures in millimeter and submillimeter single dish and interferometric observations requires the measurement of calibrated loads. The traditional mode for deriving and calibrating the T^*_A and T_{sys} temperature scales at millimeter wavelengths is the "chopper wheel" technique (Penzias & Burrus 1973; Ulich & Haas 1976). In the chopper wheel calibration system, the response of the receiver to one or two calibrated loads is combined with a measurement of the emission due to the sky to derive T^*_A and T_{sys}. In both flavours of the chopper wheel calibration technique, it is assumed that G_s and η_l are known. In the following, we will discuss the three variants of the chopper wheel calibration technique.

4.1 Generalized Two–Load Chopper Wheel

The most direct way to measure T_A^* and T_{sys} is to use the two–load chopper wheel calibration technique. As one can see by examining Equations 5, 8, and 9, two calibrated loads are required to directly measure K in Equation 5, and $T_A(sky)$ and T_{rx} in Equation 8.

A direct measure of K is derived by noting that

$$\frac{(V_{load1} - V_{offset})}{K} = f_1\left[G_s J^s_{load1} + G_i J^i_{load1}\right] + T_{rx} \quad (10)$$

$$\frac{(V_{load2} - V_{offset})}{K} = f_2\left[G_s J^s_{load2} + G_i J^i_{load2}\right] + T_{rx} \quad (11)$$

Taking the difference of these two equations and solving for K yields

$$K = \frac{V_{load1} - V_{load2}}{f_1\left[G_s J^s_{load1} + G_i J^i_{load1}\right] - f_2\left[G_s J^s_{load2} + G_i J^i_{load2}\right]} \quad (12)$$

so that

$$\boxed{(T_A^*)^{two-load} = \left(\frac{V_{source} - V_{sky}}{V_{load1} - V_{load2}}\right)\left\{\frac{f_1\left[J^s_{load1} + R_i J^i_{load1}\right] - f_2\left[J^s_{load2} + R_i J^i_{load2}\right]}{\eta_l \exp(-\tau_s)}\right\}} \quad (13)$$

The main shortcoming of the two-load chopper wheel technique is that a measurement of the atmospheric opacity in the signal sideband at the elevation of the source, τ_s, is required. This measurement is usually gotten by making a tipping scan in the direction of the source.

4.2 One–Load Chopper Wheel (Traditional Chopper Wheel)

The one-load chopper wheel technique is the simplest to implement as it requires only a chopping vane placed over the feed of the receiver. Its main shortcoming is that a model of the emission due to the sky must be used to derive T_A^* and T_{sys}. In the following, we will derive the dependence of T_A^* on the various measurable terms in a one-load chopper wheel system.

Starting with Equation 13 and substituting

$$\begin{aligned} V_{load1} &= V_{load} \\ V_{load2} &= V_{sky} \\ T_{load1} &= T_{load} \\ T_{load2} &= T_A(sky) \\ f_1 &= 1 \\ f_2 &= 1 \\ \Gamma &\equiv \frac{V_{source} - V_{sky}}{V_{load1} - V_{load2}} \end{aligned}$$

we find that

$$
\begin{aligned}
(T_A^*)^{one-load} = \quad & \frac{\Gamma}{\eta_l \exp(-\tau_s)} \Bigg[J^s_{load} - \eta_l J^s_m \left[1 - \exp(-\tau_s)\right] - (1-\eta_l)\, J^s_{spill} - \\
& \eta_l J^s_{bg} \exp(-\tau_s) + R_i \Big[J^i_{load} - \eta_l J^i_m \left[1 - \exp(-\tau_i)\right] - (1-\eta_l)\, J^i_{spill} - \\
& \eta_l J^i_{bg} \exp(-\tau_i) \Big] \Bigg]
\end{aligned} \tag{14}
$$

Note that for $T_m \simeq T_{spill} \simeq T_{load}$ and $\tau_s \simeq \tau_i$, Equation 14 is independent of τ.

A common quantity used at millimeter and submillimeter observatories which use the one-load chopper wheel technique is the "calibration temperature" T_c. In Equation 14 T_c is given by $\frac{T_A^*}{\Gamma}$.

4.3 One–Load Chopper Wheel (Semi-Transparent Vane)

A variant of the traditional chopper wheel technique uses a chopping vane which is semi-transparent at millimeter and submillimeter wavelengths. Note that this variant of the one-load chopper wheel technique is also dependent on a model of the emission due to the atmosphere.

Starting with Equation 13 and substituting

$$
\begin{aligned}
V_{load1} &= f V_{load} + (1-f) V_{sky} \\
V_{load2} &= V_{sky} \\
T_{load1} &= f T_{load} + (1-f) T_A(sky) \\
T_{load2} &= T_A(sky) \\
f_1 &= f \\
f_2 &= 1 \\
\Gamma &\equiv \frac{V_{source} - V_{sky}}{V_{load1} - V_{load2}}
\end{aligned}
$$

we find that

$$
\begin{aligned}
(T_A^*)^{one-load}_{semi-trans} = & \frac{\Gamma f}{\eta_l \exp(-\tau_s)} \Bigg[J^s_{load} - \eta_l J^s_m \left[1 - \exp(-\tau_s)\right] - (1-\eta_l)\, J^s_{spill} - \\
& \eta_l J^s_{bg} \exp(-\tau_s) + R_i \Big[J^i_{load} - \eta_l J^i_m \left[1 - \exp(-\tau_i)\right] - (1-\eta_l)\, J^i_{spill} - \\
& \eta_l J^i_{bg} \exp(-\tau_i) \Big] \Bigg]
\end{aligned} \tag{15}
$$

5 Variance of the T_A^* Scale

5.1 Generalized Two–Load Chopper Wheel

In the following, we assume that V_{load1}, V_{load2}, V_{source}, and V_{sky} can be measured exactly. We then calculate the variance of $(T_A^*)^{two-load}$ (Equation 13) with respect to the free variables J^s_{load1}, J^s_{load2}, J^i_{load1}, J^i_{load2}, R_i, η_l, τ_s, f_1, and f_2.

$$\begin{aligned}
\sigma^2(T_A^*)^{two-load} &= \sigma^2(T_{load1})\left(\frac{\partial(T_A^*)^{two-load}}{\partial T_{load1}}\right)^2 + \sigma^2(T_{load2})\left(\frac{\partial(T_A^*)^{two-load}}{\partial T_{load2}}\right)^2 + \\
&\quad \sigma^2(R_i)\left(\frac{\partial(T_A^*)^{two-load}}{\partial R_i}\right)^2 + \sigma^2(\eta_l)\left(\frac{\partial(T_A^*)^{two-load}}{\partial \eta_l}\right)^2 + \\
&\quad \sigma^2(f_1)\left(\frac{\partial(T_A^*)^{two-load}}{\partial f_1}\right)^2 + \sigma^2(f_2)\left(\frac{\partial(T_A^*)^{two-load}}{\partial f_2}\right)^2 + \\
&\quad \sigma^2(\tau_s)\left(\frac{\partial(T_A^*)^{two-load}}{\partial \tau_s}\right)^2 \qquad (16)
\end{aligned}$$

Using the partial derivatives of Equation 13 calculated in Appendix B, we find that

$$\begin{aligned}
\left(\frac{\sigma(T_A^*)^{two-load}}{(T_A^*)^{two-load}}\right)^2 &= \sigma^2(T_{load1})\left[\left(\frac{f_1}{\alpha}\right)\left((J^s_{load1})' + R_i(J^i_{load1})'\right)\right]^2 + \\
&\quad \sigma^2(T_{load2})\left[\left(\frac{f_2}{\alpha}\right)\left((J^s_{load2})' + R_i(J^i_{load2})'\right)\right]^2 + \\
&\quad \frac{\sigma^2(\eta_l)}{\eta_l^2} + \sigma^2(\tau_s) + \\
&\quad \sigma^2(R_i)\left(\frac{f_1 J^i_{load1} - f_2 J^i_{load2}}{\alpha}\right)^2 + \\
&\quad \sigma^2(f_1)\left(\frac{J^s_{load1} + R_i J^i_{load1}}{\alpha}\right)^2 + \\
&\quad \sigma^2(f_2)\left(\frac{J^s_{load2} + R_i J^i_{load2}}{\alpha}\right)^2 \qquad (17)
\end{aligned}$$

5.2 One–Load Chopper Wheel (Traditional Chopper Wheel)

In the following, we assume that V_{source}, V_{sky}, V_{load}, and T_{bg} can be measured exactly. Note also that τ_s and τ_i are correlated such that

$$\tau_s = \tau_i + \Delta\tau \qquad (18)$$

where $\Delta\tau$ is a constant which depends primarily upon the contribution due to O_2. With these assumptions, we can now calculate the variance of $(T_A^*)^{one-load}$ with respect to the free variables J_m^s, J_m^i, J_{load}^s, J_{load}^i, J_{spill}^s, J_{spill}^i, R_i, η_l, and τ_s

$$\begin{aligned}\sigma^2(T_A^*)^{one-load} &= \sigma^2(T_m)\left(\frac{\partial(T_A^*)^{one-load}}{\partial T_m}\right)^2 + \sigma^2(T_{load})\left(\frac{\partial(T_A^*)^{one-load}}{\partial T_{load}}\right)^2 + \\ &\quad \sigma^2(T_{spill})\left(\frac{\partial(T_A^*)^{one-load}}{\partial T_{spill}}\right)^2 + \sigma^2(R_i)\left(\frac{\partial(T_A^*)^{one-load}}{\partial R_i}\right)^2 + \\ &\quad \sigma^2(\eta_l)\left(\frac{\partial(T_A^*)^{one-load}}{\partial \eta_l}\right)^2 + \sigma^2(\tau_s)\left(\frac{\partial(T_A^*)^{one-load}}{\partial \tau_s}\right)^2 \end{aligned} \quad (19)$$

Using the partial derivatives of Equation 14 calculated in Appendix C, we find that

$$\begin{aligned}\left(\frac{\sigma(T_A^*)^{one-load}}{(T_A^*)^{one-load}}\right)^2 &= \sigma^2(T_m)\left\{\frac{\eta_l}{\gamma}\left[(J_m^s)'\left[\exp(-\tau_s)-1\right] + R_i(J_m^i)'\left[\exp(-\tau_i)-1\right]\right]\right\}^2 + \\ &\quad \sigma^2(T_{load})\left\{\left(\frac{1}{\gamma}\right)\left((J_{load}^s)' + R_i(J_{load}^i)'\right)\right\}^2 + \\ &\quad \sigma^2(T_{spill})\left\{\left(\frac{\eta_l - 1}{\gamma}\right)\left((J_{spill}^s)' + R_i(J_{spill}^i)'\right)\right\}^2 + \\ &\quad \sigma^2(R_i)\left[\frac{J_{load}^i - J_m^i\eta_l\left[1-\exp(-\tau_i)\right] - (1-\eta_l)J_{spill}^i - \eta_l J_{bg}^i\exp(-\tau_i)}{\gamma}\right]^2 + \\ &\quad \sigma^2(\eta_l)\left\{\frac{1}{\eta_l} + \frac{1}{\gamma}\left[J_m^s\left[1-\exp(-\tau_s)\right] - J_{spill}^s + J_{bg}^s\exp(-\tau_s) + \right.\right. \\ &\quad \left.\left. R_i\left(J_m^i\left[1-\exp(-\tau_i)\right] - J_{spill}^i + J_{bg}^i\exp(-\tau_i)\right)\right]\right\}^2 + \\ &\quad \sigma^2(\tau_s)\left[1 - \frac{\eta_l\exp(-\tau_s)}{\gamma}\left[J_m^s - J_{bg}^s + R_i\exp(\Delta\tau)\left(J_m^i - J_{bg}^i\right)\right]\right]^2 \end{aligned} \quad (20)$$

5.3 One–Load Chopper Wheel (Semi-Transparent Vane)

As was done in §5.2, we assume that V_{source}, V_{sky}, V_{load}, and T_{bg} can be measured exactly. We can now calculate the variance of $(T_A^*)_{semi-trans}^{one-load}$ with respect to the free variables J_m^s, J_m^i, J_{load}^s, J_{load}^i, J_{spill}^s, J_{spill}^i, R_i, η_l, τ_s, and f. Since $(T_A^*)_{semi-trans}^{one-load}$ differs from $(T_A^*)^{one-load}$ only by an extra term involving f, inspection of Equations 14 and 15 reveals that

$$\left(\frac{\sigma(T_A^*)_{semi-trans}^{one-load}}{(T_A^*)_{semi-trans}^{one-load}}\right)^2 = \left(\frac{\sigma(T_A^*)^{one-load}}{(T_A^*)^{one-load}}\right)^2 + \frac{\sigma^2(f)}{f^2} \quad (21)$$

6 Comparative Uncertainty of the One- and Two-Load Chopper Wheel Calibration Techniques

In Table 1 we have listed values for each term in the variance relations $\left(\frac{\sigma(T_A^*)^{one-load}}{(T_A^*)^{one-load}}\right)$ (Equation 20), $\left(\frac{\sigma(T_A^*)^{one-load}_{semi-trans}}{(T_A^*)^{one-load}_{semi-trans}}\right)$ (Equation 21), and $\left(\frac{\sigma(T_A^*)^{two-load}}{(T_A^*)^{two-load}}\right)$ (Equation 17). For these calculations we assumed

- A zenith atmospheric opacity at each frequency based on atmospheric model calculations assuming 1mm PWV on the Chajnantor site;
- Zenith opacity measurement accuracy of 1% (best) and 10% (worst).
- That the elevation of observation was 45°;
- Double sideband receiver systems;
- Mean atmospheric temperature measurement accuracy of 2% (best) and 10% (worst). The best-case value of 2% is based on an analysis of the ATM code by Cernicharo (private communication).
- Load temperatures and regulation accuracy for the two-load calibration system characteristic of those used in the BIMA prime focus calibration system. In that system, there are two temperature-regulated loads at 310 K and 400 K which couple to the receiver feed with an efficiency of about 2%. The accuracy of the absolute temperature regulation for both loads is dominated by the accuracy of the temperature sensor, which is 0.1 K (∼0.05%) (Welch, private communication).
- Equal signal and image sideband atmospheric opacities and uncertainties.
- Load coupling factor uncertainties of 0.1% (best) and 1% (worst).
- Load temperature regulation of 1% (best) and 2% (worst).

Five calculations are shown for each frequency, representing (1) best-case conditions, (2) uncertain T_m, (3) uncertain load temperatures, (4) uncertain atmospheric opacities, and (5) uncertain load coupling factors. Plots of the contributions of each error term to the total uncertainty are shown in Figures 2 and 3 (note that the uncertainties are essentially the same at 490 and 650 GHz). The conclusions from these comparisons are:

1. The most optimistic conditions lead to uncertainties of approximately 1% for the one- and two-load chopper calibration systems. The 1% uncertainty value is consistent with the results of the BIMA prime focus two-load calibration system (see Welch *et. al.* 2000).
2. All load calibration techniques are affected equally by the uncertainty in η_l. This is historically tied to the fact that the chopper wheel calibration scheme was developed for prime focus receiving systems.

3. At higher frequencies, the uncertainty in the mean atmospheric temperature and the load temperatures dominate the overall uncertainty of the one-load chopper calibration technique.

4. The accuracy of the atmospheric opacity measurement is the major uncertainty dominating the accuracy of the two-load calibration system. Atmospheric opacity should be measured to an accuracy of at least 1% to obtain <2% overall uncertainty with the two-load calibration system.

5. Accurate knowledge of the relative sideband gain (R_i) is extremely important. For example, if $\sigma(R_i) = 10\%$ rather than the standard value of 1%, the best-case uncertainty in the one- and two-load chopper calibration techniques becomes 5% at 230 GHz.

7 Conclusions

1. A two-load chopper wheel calibration system is necessary to have the potential of achieving 1% calibration uncertainty of the T_A^* temperature scale. The main drawback of the two-load calibration system is the need for an independent measurement of the atmospheric opacity τ. This measurement can be derived from a tipping scan or from a dedicated opacity monitor such as a Fourier transform spectrometer system (at each antenna) which monitors the atmospheric opacity continuously at all frequencies.

References

Holdaway, M. A. 1996, MMA Memo 149.

Kutner, M. L. & Ulich, B. L. 1981, ApJ, 250, 341.

Penzias, A. A. & Burrus, C. A. 1973, ARA&A, 11, 51

Ulich, B. L. & Haas, R. W. 1976, ApJS, 30, 247

Yun, M. S., Mangum, J. G., Bastian, T., Holdaway, M., & Welch, W. J. 1998, MMA Memo 211.

Welch, W. J., Bock, D. C.-J., Fleming, M. C., & Thornton, D. D. 2000, in *Imaging at Radio through Submillimeter Wavelengths*

Table 1: Chopper Wheel Calibration Uncertainty

$\frac{\sigma(T_m)}{T_m}$	$\frac{\sigma(T_{load})}{T_{load}}$	$\frac{\sigma(f_1)}{f_1}$	$\frac{\sigma(f_2)}{f_2}$	$\frac{\sigma(f)}{f}$	$\frac{\sigma(\tau_s)}{\tau_s}$	$\frac{\sigma(\tau_i)}{\tau_i}$	$\frac{\sigma(T_{load1})}{T_{load1}}$	$\frac{\sigma(T_{load2})}{T_{load2}}$	$\frac{\sigma(T_A^*)}{T_A^*}$ [a]		
$\nu = 230$ GHz[b]									one-load	$\frac{\text{one-load}}{\text{semi-trans}}$	two-load
$\frac{5}{268}$	$\frac{2.6}{268}$	$\frac{0.00008}{0.08}$	$\frac{0.00008}{0.08}$	$\frac{0.0005}{0.50}$	$\frac{0.0007}{0.07}$	$\frac{0.0007}{0.07}$	$\frac{0.1}{310.0}$	$\frac{0.1}{400.0}$	1.6%	1.6%	1.3%
$\frac{27}{268}$	$\frac{2.6}{268}$	$\frac{0.00008}{0.08}$	$\frac{0.00008}{0.08}$	$\frac{0.0005}{0.50}$	$\frac{0.0007}{0.07}$	$\frac{0.0007}{0.07}$	$\frac{0.1}{310.0}$	$\frac{0.1}{400.0}$	1.8%	1.8%	1.3%
$\frac{5}{268}$	$\frac{5.2}{268}$	$\frac{0.00008}{0.08}$	$\frac{0.00008}{0.08}$	$\frac{0.0005}{0.50}$	$\frac{0.0007}{0.07}$	$\frac{0.0007}{0.07}$	$\frac{0.2}{310.0}$	$\frac{0.2}{400.0}$	2.4%	2.4%	1.3%
$\frac{5}{268}$	$\frac{2.6}{268}$	$\frac{0.00008}{0.08}$	$\frac{0.00008}{0.08}$	$\frac{0.0005}{0.50}$	$\frac{0.007}{0.07}$	$\frac{0.007}{0.07}$	$\frac{0.1}{310.0}$	$\frac{0.1}{400.0}$	1.6%	1.6%	1.4%
$\frac{5}{268}$	$\frac{2.6}{268}$	$\frac{0.0008}{0.08}$	$\frac{0.0008}{0.08}$	$\frac{0.005}{0.50}$	$\frac{0.0007}{0.07}$	$\frac{0.0007}{0.07}$	$\frac{0.1}{310.0}$	$\frac{0.1}{400.0}$	1.6%	1.9%	5.6%
$\nu = 490$ GHz											
$\frac{5}{268}$	$\frac{2.6}{268}$	$\frac{0.00008}{0.08}$	$\frac{0.00008}{0.08}$	$\frac{0.0005}{0.50}$	$\frac{0.01}{1.1}$	$\frac{0.01}{1.1}$	$\frac{0.1}{310.0}$	$\frac{0.1}{400.0}$	5.6%	5.6%	1.6%
$\frac{27}{268}$	$\frac{2.6}{268}$	$\frac{0.00008}{0.08}$	$\frac{0.00008}{0.08}$	$\frac{0.0005}{0.50}$	$\frac{0.01}{1.1}$	$\frac{0.01}{1.1}$	$\frac{0.1}{310.0}$	$\frac{0.1}{400.0}$	20.3%	20.3%	1.6%
$\frac{5}{268}$	$\frac{5.2}{268}$	$\frac{0.00008}{0.08}$	$\frac{0.00008}{0.08}$	$\frac{0.0005}{0.50}$	$\frac{0.01}{1.1}$	$\frac{0.01}{1.1}$	$\frac{0.2}{310.0}$	$\frac{0.2}{400.0}$	7.5%	7.5%	1.6%
$\frac{5}{268}$	$\frac{2.6}{268}$	$\frac{0.00008}{0.08}$	$\frac{0.00008}{0.08}$	$\frac{0.0005}{0.50}$	$\frac{0.1}{1.1}$	$\frac{0.1}{1.1}$	$\frac{0.1}{310.0}$	$\frac{0.1}{400.0}$	5.6%	5.6%	10.1%
$\frac{5}{268}$	$\frac{2.6}{268}$	$\frac{0.0008}{0.08}$	$\frac{0.0008}{0.08}$	$\frac{0.005}{0.50}$	$\frac{0.01}{1.1}$	$\frac{0.01}{1.1}$	$\frac{0.1}{310.0}$	$\frac{0.1}{400.0}$	5.6%	5.7%	5.6%
$\nu = 650$ GHz											
$\frac{5}{268}$	$\frac{2.6}{268}$	$\frac{0.00008}{0.08}$	$\frac{0.00008}{0.08}$	$\frac{0.0005}{0.50}$	$\frac{0.01}{1.1}$	$\frac{0.01}{1.1}$	$\frac{0.1}{310.0}$	$\frac{0.1}{400.0}$	5.7%	5.7%	1.6%
$\frac{27}{268}$	$\frac{2.6}{268}$	$\frac{0.00008}{0.08}$	$\frac{0.00008}{0.08}$	$\frac{0.0005}{0.50}$	$\frac{0.01}{1.1}$	$\frac{0.01}{1.1}$	$\frac{0.1}{310.0}$	$\frac{0.1}{400.0}$	20.6%	20.6%	1.6%
$\frac{5}{268}$	$\frac{5.2}{268}$	$\frac{0.00008}{0.08}$	$\frac{0.00008}{0.08}$	$\frac{0.0005}{0.50}$	$\frac{0.01}{1.1}$	$\frac{0.01}{1.1}$	$\frac{0.2}{310.0}$	$\frac{0.2}{400.0}$	7.5%	7.5%	1.6%
$\frac{5}{268}$	$\frac{2.6}{268}$	$\frac{0.00008}{0.08}$	$\frac{0.00008}{0.08}$	$\frac{0.0005}{0.50}$	$\frac{0.1}{1.1}$	$\frac{0.1}{1.1}$	$\frac{0.1}{310.0}$	$\frac{0.1}{400.0}$	5.7%	5.7%	10.1%
$\frac{5}{268}$	$\frac{2.6}{268}$	$\frac{0.0008}{0.08}$	$\frac{0.0008}{0.08}$	$\frac{0.005}{0.50}$	$\frac{0.01}{1.1}$	$\frac{0.01}{1.1}$	$\frac{0.1}{310.0}$	$\frac{0.1}{400.0}$	5.7%	5.8%	5.6%

[a] All calculations assume $\frac{\sigma(R_i)}{R_i} = \frac{0.01}{1.0}$, $\frac{\sigma(T_{spill})}{T_{spill}} = \frac{1}{0.95T_m}$, and $\frac{\sigma(\eta_l)}{\eta_l} = \frac{0.01}{0.98}$.

[b] The five sample calculations at each frequency shown represent best, uncertain T_m, uncertain T_{load}, $T_{load,1}$, $T_{load,2}$, uncertain τ_s and τ_i, and uncertain f_1, f_2, and f.

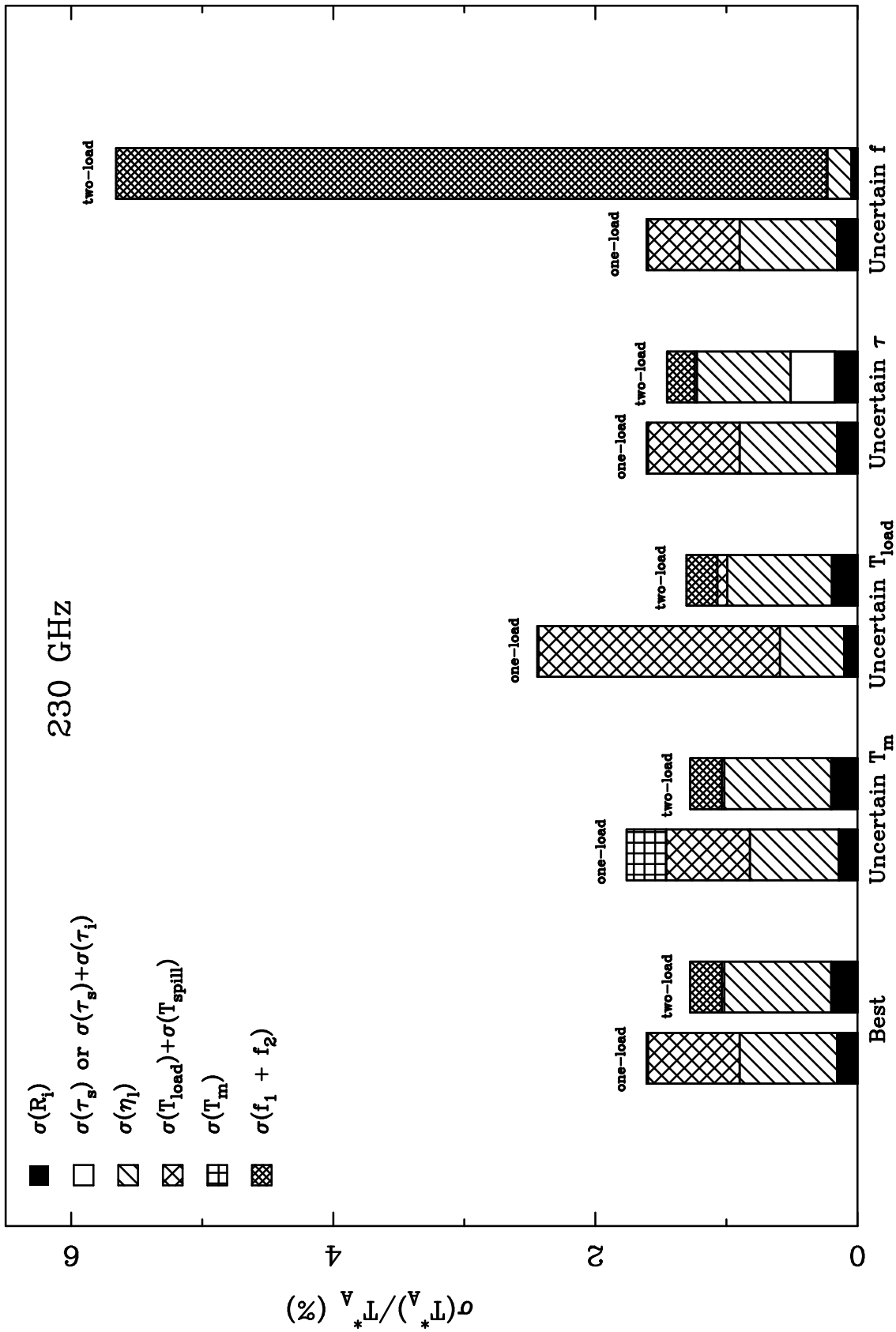

Figure 2: Chopper wheel uncertainties for 230 GHz.

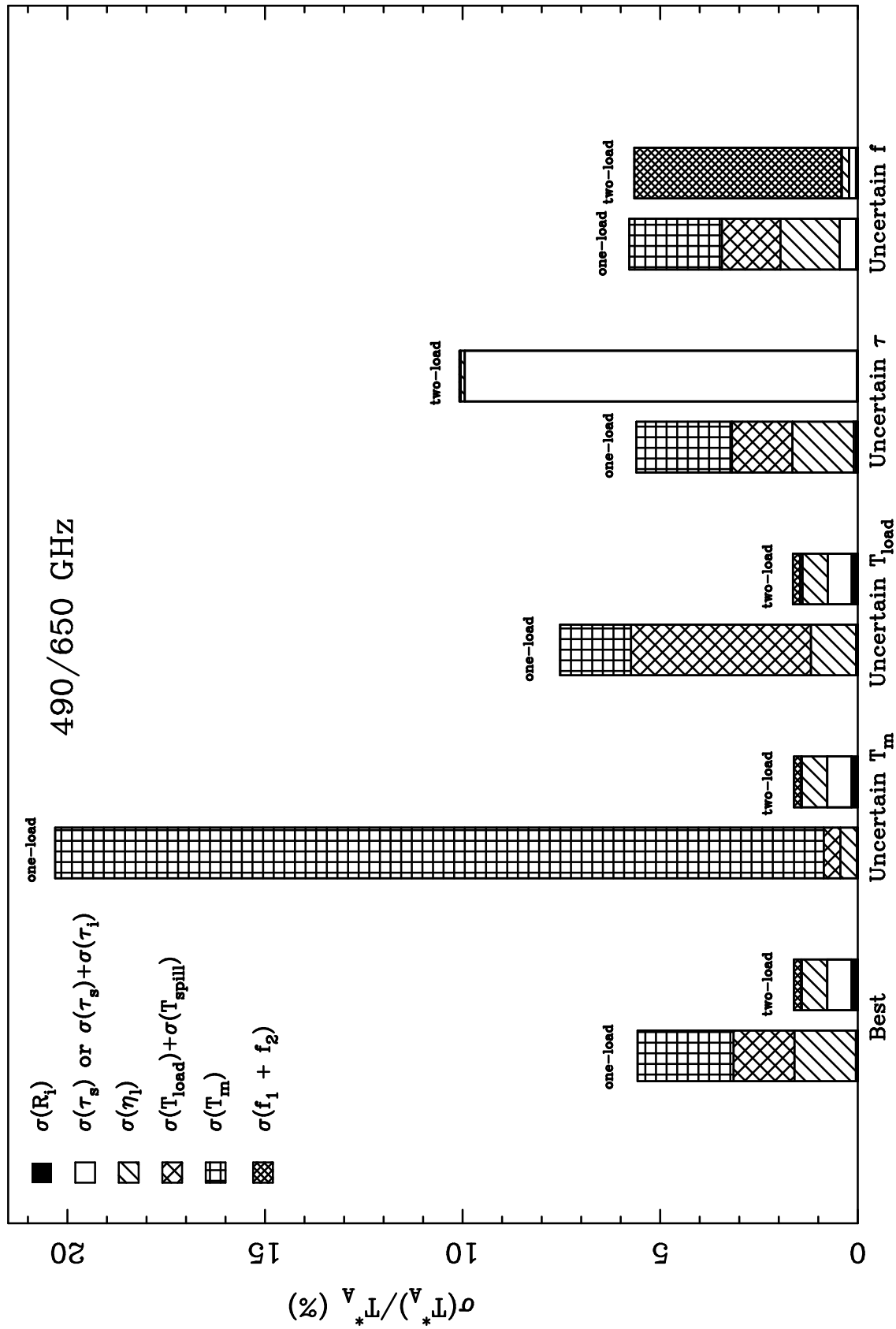

Figure 3: Chopper wheel uncertainties for 490/650 GHz.

A Definitions

Planck Equation: Note that the equivalent Rayleigh-Jeans temperature of the point on the Planck blackbody curve corresponding to the frequency ν, and its derivative with respect to temperature, are given by

$$J_T^{\nu_{sb}} = \frac{\frac{h\nu_{sb}}{k}}{\exp\left(\frac{h\nu_{sb}}{kT}\right) - 1} \tag{22}$$

$$\begin{aligned} (J_T^{\nu_{sb}})' &= \frac{\partial J_T^{\nu_{sb}}}{\partial T} \\ &= \left(\frac{h\nu_{sb}}{kT}\right)^2 \frac{\exp\left(\frac{h\nu_{sb}}{kT}\right)}{\left[\exp\left(\frac{h\nu_{sb}}{kT}\right) - 1\right]^2} \end{aligned} \tag{23}$$

Temperatures

T_{rx} is the receiver DSB noise temperature;

T_{load} (J_{load}) is the temperature of a calibration load;

T_m (J_m) is the mean atmospheric temperature;

T_{spill} (J_{spill}) is the spillover temperature;

T_{bg} (J_{bg}) is the cosmic background temperature;

T_{sky}^{cold} $(J_{sky-cold}) = \eta_l \eta_{fss} T_m \left[1 - \exp(-\tau)\right]$ is the temperature due to sky emission which terminates in the forward hemisphere;

T_{sky}^{hot} $(J_{sky-hot}) = \eta_l(1-\eta_{fss})T_m\left[1-\exp(-\tau)\right]$ is the temperature due to sky emission which terminates in the rear hemisphere;

T_{ant} $(J_{ant}) = (1-\eta_l)T_{spill}$ is the temperature of the antenna;

$T_A(sky)$ $(J_{A-sky}) = T_{sky}^{cold} + T_{sky}^{hot} + T_{ant} + \eta_l T_{bg}\exp(-\tau) = \eta_l T_m\left[1-\exp(-\tau)\right] + (1-\eta_l)T_{spill} + \eta_l T_{bg}\exp(-\tau)$ is the antenna temperature due to sky emission in the signal or image sideband;

$T_A(source)$ is the antenna temperature due to source emission;

Other

ν_s is the sky frequency in the signal sideband;

ν_i is the sky frequency in the image sideband;

η_l is the rear spillover, blockage, scattering, and ohmic efficiency;

η_{fss} is the forward spillover efficiency;

τ_s is the atmospheric optical depth in the signal sideband;

τ_i is the atmospheric optical depth in the image sideband;

G_s is the receiver gain in the signal sideband ($G_s = \frac{1}{1+R_i}$);

G_i is the receiver gain in the image sideband ($G_i = \frac{R_i}{1+R_i}$);

$R_i \equiv \frac{G_i}{G_s}$;

K is the proportionality constant between total power voltage and equivalent temperature;

V is the measured voltage from the receiver, which is proportional to the equivalent temperature of the measurement (T) given by the Planck equation;

V_{offset} is the measured DC offset voltage;

f is the fraction of the receiver beam filled by a load.

B Generalized Two–Load Chopper Wheel Partial Derivatives

$$\alpha \equiv f_1\left[J^s_{load1} + R_i J^i_{load1}\right] - f_2\left[J^s_{load2} + R_i J^i_{load2}\right] \tag{24}$$

$$\begin{aligned}
\frac{\partial (T^*_A)^{two-load}}{\partial T_{load1}} &= \frac{\partial (T^*_A)^{two-load}}{\partial J^s_{load1}} \frac{\partial J^s_{load1}}{\partial T_{load1}} + \frac{\partial (T^*_A)^{two-load}}{\partial J^i_{load1}} \frac{\partial J^i_{load1}}{\partial T_{load1}} \\
&= \frac{f_1}{\alpha}\left((J^s_{load1})' + R_i (J^i_{load1})'\right)(T^*_A)^{two-load} && (25) \\
\frac{\partial (T^*_A)^{two-load}}{\partial T_{load2}} &= \frac{\partial (T^*_A)^{two-load}}{\partial J^s_{load2}} \frac{\partial J^s_{load2}}{\partial T_{load2}} + \frac{\partial (T^*_A)^{two-load}}{\partial J^i_{load2}} \frac{\partial J^i_{load2}}{\partial T_{load2}} \\
&= -\frac{f_2}{\alpha}\left((J^s_{load2})' + R_i (J^i_{load2})'\right)(T^*_A)^{two-load} && (26) \\
\frac{\partial (T^*_A)^{two-load}}{\partial \eta_l} &= -\frac{(T^*_A)^{two-load}}{\eta_l} && (27) \\
\frac{\partial (T^*_A)^{two-load}}{\partial \tau_s} &= (T^*_A)^{two-load} && (28) \\
\frac{\partial (T^*_A)^{two-load}}{\partial R_i} &= \frac{\left[f_1 J^i_{load1} - f_2 J^i_{load2}\right](T^*_A)^{two-load}}{\alpha} && (29) \\
\frac{\partial (T^*_A)^{two-load}}{\partial f_1} &= \frac{\left[J^s_{load1} + R_i J^i_{load1}\right](T^*_A)^{two-load}}{\alpha} && (30) \\
\frac{\partial (T^*_A)^{two-load}}{\partial f_2} &= -\frac{\left[J^s_{load2} + R_i J^i_{load2}\right](T^*_A)^{two-load}}{\alpha} && (31)
\end{aligned}$$

C One–Load Chopper Wheel Partial Derivatives

$$\begin{aligned}
\gamma &\equiv J^s_{load} - J^s_m \eta_l \left[1 - \exp(-\tau_s)\right] - (1-\eta_l)\, J^s_{spill} - \eta_l J^s_{bg} \exp(-\tau_s) + \\
&\quad R_i \left[J^i_{load} - J^i_m \eta_l \left[1 - \exp(-\tau_i)\right] - (1-\eta_l)\, J^i_{spill} - \eta_l J^i_{bg} \exp(-\tau_i)\right] \qquad (32)\\
\tau_s &= \tau_i + \Delta\tau;\ \Delta\tau = \text{constant} \qquad (33)
\end{aligned}$$

$$\begin{aligned}
\frac{\partial (T^*_A)^{one-load}}{\partial T_m} &= \frac{\partial (T^*_A)^{one-load}}{\partial J^s_m}\frac{\partial J^s_m}{\partial T_m} + \frac{\partial (T^*_A)^{one-load}}{\partial J^i_m}\frac{\partial J^i_m}{\partial T_m} \\
&= \frac{\eta_l}{\gamma}\left[\left[\exp(-\tau_s) - 1\right](J^s_m)' + R_i (J^i_m)'\left[\exp(-\tau_i) - 1\right]\right](T^*_A)^{one-load} \qquad (34)\\
\frac{\partial (T^*_A)^{one-load}}{\partial T_{load}} &= \frac{\partial (T^*_A)^{one-load}}{\partial J^s_{load}}\frac{\partial J^s_{load}}{\partial T_{load}} + \frac{\partial (T^*_A)^{one-load}}{\partial J^i_{load}}\frac{\partial J^i_{load}}{\partial T_{load}} \\
&= \frac{(J^s_{load})' + R_i (J^i_{load})'}{\gamma}(T^*_A)^{one-load} \qquad (35)\\
\frac{\partial (T^*_A)^{one-load}}{\partial T_{spill}} &= \frac{\partial (T^*_A)^{one-load}}{\partial J^s_{spill}}\frac{\partial J^s_{spill}}{\partial T_{spill}} + \frac{\partial (T^*_A)^{one-load}}{\partial J^i_{spill}}\frac{\partial J^i_{spill}}{\partial T_{spill}} \\
&= \frac{(\eta_l - 1)}{\gamma}\left((J^s_{spill})' + R_i (J^i_{spill})'\right)(T^*_A)^{one-load} \qquad (36)\\
\frac{\partial (T^*_A)^{one-load}}{\partial \eta_l} &= -(T^*_A)^{one-load}\left[\frac{1}{\eta_l} + \frac{1}{\gamma}\left[J^s_m\left[1 - \exp(-\tau_s)\right] - J^s_{spill} + J^s_{bg}\exp(-\tau_s) + \right.\right. \\
&\quad \left.\left. R_i\left[J^i_m\left[1 - \exp(-\tau_i)\right] - J^i_{spill} + J^i_{bg}\exp(-\tau_i)\right]\right]\right] \qquad (37)\\
\frac{\partial (T^*_A)^{one-load}}{\partial \tau_s} &= (T^*_A)^{one-load}\left[1 - \frac{\eta_l \exp(-\tau_s)}{\gamma}\left[J^s_m - J^s_{bg} + \right.\right. \\
&\quad \left.\left. R_i \exp(\Delta\tau)\left(J^i_m - J^i_{bg}\right)\right]\right] \qquad (38)\\
\frac{\partial (T^*_A)^{one-load}}{\partial R_i} &= \frac{(T^*_A)^{one-load}}{\gamma}\left[J^i_{load} - J^i_m \eta_l \left[1 - \exp(-\tau_i)\right] - (1-\eta_l) J^i_{spill} - \right. \\
&\quad \left. \eta_l J^i_{bg}\exp(-\tau_i)\right] \qquad (39)\\
\frac{\partial (T^*_A)^{one-load}_{semi-trans}}{\partial f} &= \frac{(T^*_A)^{one-load}_{semi-trans}}{f} \qquad (40)
\end{aligned}$$

D Temperature Scales and Telescope Efficiencies

The calibration mode used for essentially all spectral line observations at most millimeter and submillimeter observatories is the chopper wheel method (see Ulich & Haas 1976). The chopper wheel technique corrects for atmospheric attenuation and several telescope losses. In the following, I describe a variety of temperature scales used at many millimeter and submillimeter observatories.

D.1 Definitions

In the following I define the terms used in the subsequent temperature scale and telescope efficiency discussion. I have tried to adopt a similar nomenclature to that used in Kutner & Ulich (1981). Note that throughout this discussion when I refer to a "temperature" I am actually referring to the effective source radiation temperature $J(\nu, T)$, which is defined by Equation 22.

General Terms

$\Omega_s \equiv$ Solid angle subtended by the source
$\Omega_d \equiv$ Solid angle subtended by the central diffraction beam pattern of the telescope
$\Omega \equiv$ Solid angle on the sky
$\Psi \equiv$ Direction angle on the sky
$P_n \equiv$ Normalized antenna power pattern
$P_{ng} \equiv$ Normalized Gaussian antenna power pattern
$B_n \equiv$ Normalized source brightness distribution
$A \equiv$ Airmass toward which the measurement is made
$\tau_0 \equiv$ Atmospheric optical depth at the zenith
$G \equiv$ Maximum antenna gain

Efficiencies

$$\eta_r \equiv \text{Radiative efficiency}$$
$$\equiv \frac{G}{4\pi}\iint_{4\pi} P_n(\Omega)d\Omega \tag{41}$$

$$\eta_{rss} \equiv \text{Rearward scattering and spillover efficiency}$$
$$\equiv \frac{\iint_{2\pi} P_n(\Omega)d\Omega}{\iint_{4\pi} P_n(\Omega)d\Omega} \tag{42}$$

$$\eta_l \equiv \eta_r\eta_{rss} \tag{43}$$

$$\eta_{fss} \equiv \text{Forward scattering and spillover efficiency}$$
$$\equiv \frac{\iint_{\Omega_d} P_n(\Omega)d\Omega}{\iint_{2\pi} P_n(\Omega)d\Omega} \tag{44}$$

$$\eta_{mb} \equiv \text{Main beam efficiency}$$
$$\equiv \frac{\iint_{4\pi} P_{ng}(\Omega)d\Omega}{\iint_{4\pi} P_n(\Omega)d\Omega} \tag{45}$$

$$\eta_{cmb} \equiv \text{Efficiency at which the source couples to the main diffraction beam of the telescope}$$
$$\equiv \frac{\iint_{\Omega_s} P_n(\Psi-\Omega)B_n(\Psi)d\Psi}{\iint_{4\pi} P_{ng}(\Omega)d\Omega} \tag{46}$$

$$\eta_c \equiv \text{Efficiency at which the source couples to the telescope beam}$$
$$\equiv \eta_{cmb}\eta_{mb}$$
$$\equiv \frac{\iint_{\Omega_s} P_n(\Psi-\Omega)B_n(\Psi)d\Psi}{\iint_{4\pi} P_n(\Omega)d\Omega}[12pt] \tag{47}$$

Temperatures

$T_R \equiv$ Source radiation temperature

$$\begin{aligned} T_A &\equiv \text{Observed source antenna temperature} \\ &\equiv \frac{GT_R}{4\pi}\exp(-A\tau_0)\iint_{\Omega_s} P_n(\Psi-\Omega)B_n(\Psi)d\Psi \end{aligned} \tag{48}$$

$$\begin{aligned} T'_A &\equiv \text{Observed source antenna temperature corrected for atmospheric attenuation} \\ &\equiv T_A\exp(A\tau_0) \end{aligned} \tag{49}$$

$$\begin{aligned} T^*_A &\equiv \text{Observed source antenna temperature corrected for atmospheric attenuation,} \\ &\quad \text{radiative loss, and rearward scattering and spillover} \\ &\equiv \frac{T'_A}{\eta_r\eta_{rss}} \end{aligned} \tag{50}$$

$$\begin{aligned} T^*_R &\equiv \text{Observed source antenna temperature corrected for atmospheric attenuation,} \\ &\quad \text{radiative loss, and rearward and forward scattering and spillover}[1] \\ &\equiv \frac{T^*_A}{\eta_{fss}} \end{aligned} \tag{51}$$

$$\begin{aligned} \Delta T_R &\equiv \text{Source radiation temperature excluding any background emission} \\ &\quad \text{(like the cosmic microwave background emission)} \\ &\equiv T_R - T_{bg} \\ &\equiv \frac{T^*_R}{\eta_c} \end{aligned} \tag{52}$$

$$\begin{aligned} T_{mb} &\equiv \text{Source brightness temperature as measured by the main diffraction beam} \\ &\quad \text{of the telescope} \\ &\equiv \eta_{cmb}\Delta T_R \end{aligned} \tag{53}$$

D.2 Relations Between Temperature Scales

We can now combine the definitions above to derive the relations between the physical measurements and the temperature scales used at many millimeter and submillimeter observatories. Combining the equations above, we can relate the source temperature corrected for atmospheric attenuation (T'_A) to many of the antenna and source temperatures:

[1] T^*_R can also be defined as the source brightness temperature corrected for atmospheric attenuation, radiative loss, and rearward and forward scattering and spillover if the source is equal to or larger than the main diffraction beam.

$$
\begin{aligned}
T'_A &= \eta_r \eta_{rss} \eta_{fss} \eta_c \Delta T_R && (54)\\
&= \eta_l \eta_{fss} T^*_R && (55)\\
&= \eta_l T^*_A && (56)\\
&= \eta_{mb} T_{mb} && (57)
\end{aligned}
$$

D.3 Telescope Efficiency Measurements

Telescope efficiencies are normally calculated using a measurement of the continuum brightness of a planet (for η_{mb}) or the Moon (for η_{fss}). In the following I give the relations used to calculate several telescope efficiencies. Since the source coupling between a disk source like the planets and a Gaussian telescope beam is given by:

$$
\eta_{cmb} = 1 - \exp\left[-\ln(2)\left(\frac{\theta_s}{\theta_B}\right)^2\right] \tag{58}
$$

I will use this term in the efficiency equation derivations given below.

D.3.1 Corrected Main Beam Efficiency

The efficiency factor which converts the T^*_A scale to the T_{mb} scale is given by:

$$
\begin{aligned}
\eta_m &= \frac{T^*_A}{T_{mb}} \\
&= \frac{T^*_A}{(T_R - T_{bg})\left\{1 - \exp\left[-\ln(2)\left(\frac{\theta_s}{\theta_B}\right)^2\right]\right\}} && (59)
\end{aligned}
$$

One can also calculate η_m using the Ruze equation:

$$
\eta_m = \left[1 + \frac{A_e \theta_e^2}{A_m \theta_m^2}\right]^{-1} \tag{60}
$$

given that:

$$
\begin{aligned}
\theta_e &= 2\sqrt{\ln(2)}\frac{\lambda}{\pi c_\sigma} && (61)\\
\theta_m &= 1.22\frac{\lambda}{D} && (62)\\
\frac{A_e}{A_m} &= \frac{1}{\eta_{a0}}\left[\frac{2c_\sigma}{D}\right]^2 \left[exp(\delta^2) - 1\right] && (63)
\end{aligned}
$$

where λ is the wavelength of observation, c_σ is the correlation scale size of the surface deviations, η_{a0} is the zero wavelength aperture efficiency, and δ is the surface accuracy.

D.3.2 Main Beam Efficiency

The efficiency factor which converts any source antenna measurement to the T_{mb} scale is given by:

$$\begin{aligned} \eta_{mb} &= \frac{T'_A}{T_{mb}} \\ &= \frac{\eta_l T^*_A}{(T_R - T_{bg}) \left\{ 1 - \exp\left[-\ln(2) \left(\frac{\theta_s}{\theta_B} \right)^2 \right] \right\}} \end{aligned} \tag{64}$$